

## LETTERS

# Effect of phase transitions on compressional-wave velocities in the Earth's mantle

Li Li<sup>1</sup> & Donald J. Weidner<sup>1</sup>

The velocities of seismic waves in the Earth are governed by the response of the constituent mineral assemblage to perturbations in pressure and stress. The effective bulk modulus is significantly lowered if the pressure of the seismic wave drives a volume-reducing phase transformation<sup>1,2</sup>. A comparison between the amount of time required by phase transitions to reach equilibrium and the sampling period thus becomes crucial in defining the softening and attenuation of compressional waves within such a two-phase zone<sup>3</sup>. These phenomena are difficult to assess experimentally, however, because data at conditions appropriate to the Earth's deep interior are required. Here we present synchrotron-based experimental data that demonstrate softening of the bulk modulus within the two-phase loop of olivine–ringwoodite on a timescale of 100 s. If the amplitude of the pressure perturbation and the grain size are scaled to those expected in the Earth, the compressional-wave velocities within the discontinuities at 410, 520 and, possibly, 660 km are likely to be significantly lower than otherwise expected. The generalization of these observations to aluminium-controlled phase transitions raises the possibility of large velocity perturbations throughout the upper 1,000 km of the mantle.

The current view of the radial seismic structure of the mantle consists of smooth velocity variations punctuated by discontinuities at 410, 520, and 660 km (ref. 4), which are thought to be caused by the olivine–wadsleyite–ringwoodite–perovskite phase transitions<sup>5,6</sup>. However, complexities arise from the possible relaxation of the bulk modulus caused by phase transitions<sup>1</sup> in regions of coexisting high- and low-pressure phases. The olivine phase transitions have finite widths owing to the partitioning of iron and magnesium between coexisting phases<sup>7,8</sup>. Some of the 'smooth' zones consist of coexisting high- and low-pressure phases of pyroxene–garnet–perovskite, which tend to have broad two-phase zones that are controlled by the partitioning of aluminium between coexisting phases<sup>9</sup>. In the regions with coexisting high- and low-pressure phases, the equilibrium bulk modulus,  $K_{\text{eq}}$ , will be considerably relaxed because a pressure change will induce a volume change that is the result of the pressure-induced phase transformation:

$$-\frac{\delta V}{V} = -\frac{\delta P}{\Delta P_{\text{tran}}}\left(\frac{\Delta V}{V}\right)_{\text{tran}} + \frac{\delta P}{K_{\text{elas}}} = \delta P\left(\frac{1}{K_{\text{tran}}} + \frac{1}{K_{\text{elas}}}\right) = \frac{\delta P}{K_{\text{cq}}}$$

where  $\Delta P_{\text{tran}}$  is the width of the two-phase zone,  $(\Delta V/V)_{\text{tran}}$  is the proportional volume change associated with the transformation and  $K_{\text{elas}}$  is the elastic unrelaxed bulk modulus of the two-phase aggregate when no phase transition occurs. Whether  $K_{\text{cq}}$  or  $K_{\text{elas}}$  defines the P-wave velocity depends on whether the kinetics of the transformation occur on a timescale respectively shorter or longer than the period of the seismic wave.

Figure 1 illustrates the effect on the P-wave velocity of transition-induced relaxation for a pyrolitic Earth<sup>10,11</sup> with an adiabatic temperature gradient<sup>12</sup>. Figure 1a illustrates the unrelaxed elastic system.

Figure 1b shows the relaxed system with only the olivine transforming. Figure 1c is similar to Fig. 1b, but both olivine and pyroxene reach equilibrium. Also illustrated in Fig. 1c is the preliminary reference Earth model<sup>3</sup>. It is noteworthy that this model lies between the relaxed and unrelaxed systems and is closest to the unrelaxed velocity in regions where no phase transitions occur. On the basis of our experimental results, we argue that the Earth most likely samples a significant fraction of the relaxed system resulting in a reduced P-wave velocity, but with little bulk attenuation.

The crucial issue is the timescale for the system undergoing phase transitions to reach equilibrium, in comparison with the period of seismic waves<sup>1</sup>. Kinetics rates are often attributed to nucleation of the new phase and growth of the new phase. As both phases coexist, nucleation is probably not important here. Growth requires that the composition of the region that is becoming the new phase change from one side of the controlling binary loop to the other, thus requiring diffusion. For the olivine system, iron and magnesium must exchange<sup>13</sup> by several per cent. The rate of this diffusion process defines one timescale ( $\tau_1$ ) of the transformation. For times longer than  $\tau_1$ , some transformation will occur. Complete transformation requires that the region furthest from the transforming zone equilibrate iron or magnesium with the transforming zone<sup>2,14</sup>, and defines a second timescale ( $\tau_2$ ). There is probably a range of characteristic

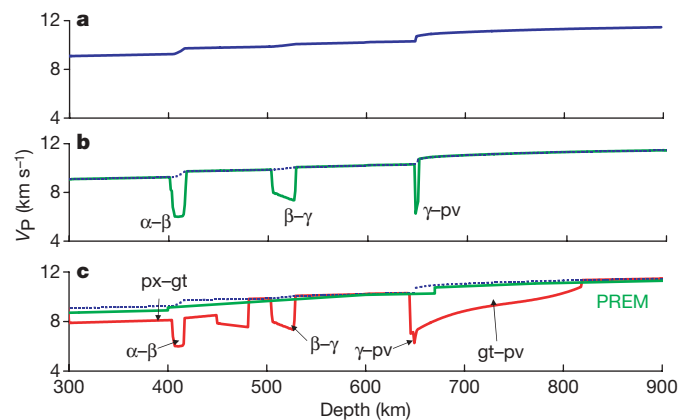


**Figure 1 | Calculated P-wave velocities ( $V_p$ ) versus depth in the Earth using pyrolite composition and adiabatic gradient<sup>8</sup>.** **a**, Here the measurement time is much less than the shortest characteristic time (which we estimate to be  $<10^{-2}$  s for P waves). **b**, Here we assume total phase equilibrium for olivine phases (green line; the blue line is the same as in **a**). **c**, Same as **b** except total equilibrium for pyroxene–garnet–perovskite transitions is also assumed (red line). The preliminary reference Earth model<sup>3</sup> (PREM) is included. Plots in **b** and **c** are calculated from the depth derivative of the density model. The density model is derived from the phase equilibria and equations of state for pyrolite minerals<sup>10</sup>.  $\alpha$ , olivine;  $\beta$ , wadsleyite;  $\gamma$ , ringwoodite; pv, perovskite; px, pyroxene; gt, garnet.

<sup>1</sup>Mineral Physics Institute Department of Geosciences, Stony Brook University, Stony Brook, New York 11794, USA.

times between  $\tau_1$  and  $\tau_2$  in the real system, yielding progressively more transformation for times between these bounds.

Equilibrium also requires heat diffusion. If latent heat does not diffuse from the system, the amount of relaxation of the bulk modulus is reduced by about one-half for the olivine system, but by very little for the pyroxene system. The timescale for heat flow thereby also enters the conditions for equilibrium<sup>15</sup>, but will not be discussed here. The characteristic time depends on the diffusion length,  $x$ , by  $\tau = x^2/D$  (ref. 2), where  $D$  is the appropriate diffusion coefficient. As pointed out in ref. 2,  $x \approx (d/3)\delta P/\Delta P_{\text{tran}}$ , where  $x$  is a transformed rim on a grain of size  $d$ . A smaller pressure perturbation  $\delta P$  will transform a smaller amount of material, thus reducing  $x$  and  $\tau_1$ . For seismic waves<sup>2</sup>, with  $\delta P$  of roughly  $10^{-7}$  GPa,  $\Delta P_{\text{tran}}$  of 0.3 GPa (width of the olivine–wadsleyite two-phase loop),  $d$  of 1 cm and  $D$  of  $10^{-15} \text{ m}^2 \text{ s}^{-1}$  for iron–magnesium exchange<sup>13</sup>,  $\tau_1$  is approximately  $10^{-2}$  s. Timescale  $\tau_2$ , which characterizes the longest diffusion distance for complete equilibrium, can reach values of  $10^{11}$  s if the diffusion path is as long as 1 cm. This implies that seismic waves, with periods between 1 and 1,000 s, will at least partially drive the phase transition and will exhibit partially relaxed velocities. If the seismic timescale were the same as the characteristic time, we would expect an associated attenuation. For the conditions outlined here, we conclude that the seismic velocities are partially relaxed, but with little or no attenuation.

In the laboratory, with values of  $\delta P$  at the gigapascal level and grains sizes of a few micrometres, we expect  $\tau_1$  to be of the order of 1,000 s. Furthermore, we expect that these characteristic times are reasonably appropriate for the olivine–wadsleyite–ringwoodite transformations as well as the pyroxene–garnet–perovskite transformations. Aluminium diffusion controls the two-phase region of the latter system. Although aluminium diffusion data are not available, gallium diffusion in garnets suggests characteristic times similar to those for the iron–magnesium exchange in olivine<sup>16</sup>. Thus, the characteristic times in Fig. 1c may be similar to those in Fig. 1b. However, a recent study<sup>17</sup> reported diffusion coefficients for the iron–magnesium exchange of  $10^{-21} \text{ m}^2 \text{ s}^{-1}$  for perovskite. This increases the characteristic time of the ringwoodite-to-perovskite transition by six orders of magnitude, and possibly out of the seismic band.

Testing this model by quantifying this phenomenon in the laboratory has been limited by the challenge of creating the appropriate pressure–temperature environment and simultaneously measuring elastic properties and attenuation of the bulk modulus at seismic frequencies. Use of the deformation DIA high-pressure system<sup>18</sup> on a synchrotron X-ray source has provided a new opportunity to pursue these goals<sup>19</sup>. Here we report two types of experiment on an olivine sample, of composition  $\text{Fa}_{70}$  (Fa, fayalite), which is used to ensure a wide two-phase loop between olivine and ringwoodite. In the first set of experiments, the time-resolved transformation between olivine and ringwoodite was defined by the X-ray diffraction pattern after a change in the pressure or temperature conditions altered the equilibrium proportions of the two phases. In the other measurements, the olivine sample ( $\sim 10\text{-}\mu\text{m}$  grain size) and an aluminium oxide reference were enclosed in a silver capsule which was placed in a high-pressure cell. At high pressure and temperature (up to 15 GPa, 1,700 K), a sinusoidal uniaxial stress is applied to the sample, inducing strains of  $10^{-2}$ – $10^{-5}$ . We measured stress–strain phase and amplitude relationships, resolved using X-ray radiation, for frequencies of 1–100 mHz. Details of the experimental procedures are reported elsewhere<sup>19</sup>.

Figure 2 shows a typical evolution of the volume per cent of the phases as a function of time after a new set of equilibrium conditions has been established. The fitted curve indicates a characteristic time of about 4,000 s. This is consistent with diffusion being the controlling process, with a value for  $D$  of  $10^{-15} \text{ m}^2 \text{ s}^{-1}$  for iron–magnesium exchange<sup>13</sup> and a characteristic length of  $2 \mu\text{m}$ , which would suggest that about half of the material undergoes transformation (with  $10 \mu\text{m}$

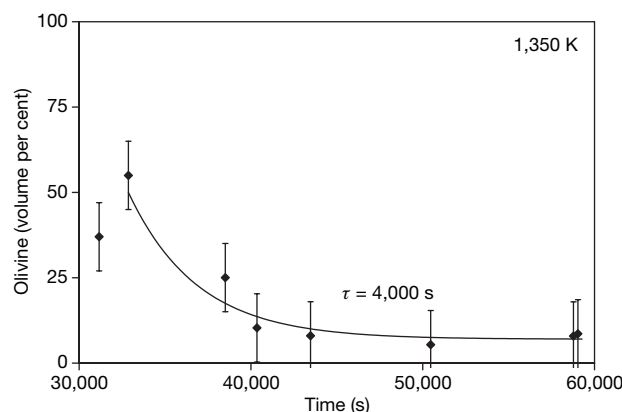


**Figure 2 | Example of the olivine content versus time, from X-ray diffraction observations.** The temperature reached 1,350 K at 33,000 s. Olivine transforms to spinel with time. The decay curve has a characteristic time of 4,000 s. These data are consistent with iron–magnesium diffusion being the dominant process, with a diffusivity of  $10^{-15} \text{ m}^2 \text{ s}^{-1}$  and a diffusion length of  $2 \mu\text{m}$ . These results support the bulk attenuation observed during loading with a period of 1,000 s (Fig. 3) and the softening observed at low amplitudes and shorter periods (Fig. 4). Run number 30; error bars, 1 s.d.

grains). This is consistent with the model described above and with previous studies on olivine phase kinetics<sup>20</sup>.

Attenuation is expected when the characteristic time is comparable to the oscillation period. Figure 3a shows one cycle of a 1,000-s oscillation, where stress (derived from the strain of the reference material) is plotted against strain of the sample. The hysteresis loop indicates energy loss in the cycle. Figure 3b shows the hysteresis loop for the same condition at a slightly lower temperature, where only the ringwoodite phase was stable as indicated by the diffraction pattern.

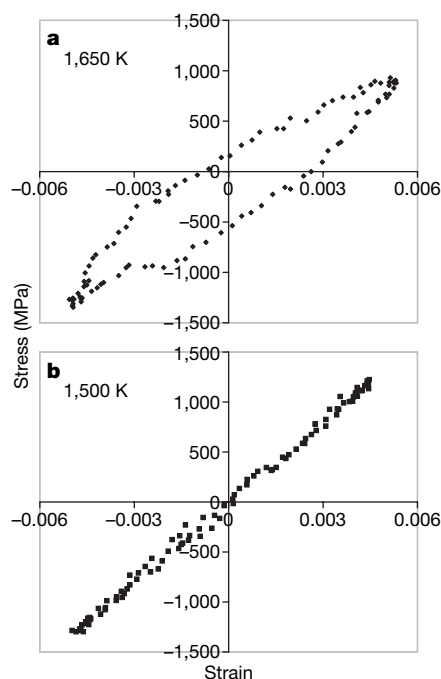


**Figure 3 | Stress versus strain for one cycle during sinusoidal loading with period of 1,000 s.** a, At 1,650 K both olivine and ringwoodite coexist in approximately equal amounts, as demonstrated by X-ray diffraction. The resulting Q factor is about five. b, At 1,500 K, X-ray diffraction indicates that ringwoodite dominates the sample. The Q factor is indistinguishable from infinity. The area inside the hysteresis loop is the energy loss during one cycle. We conclude that the phase transition is responsible for the energy dissipation.

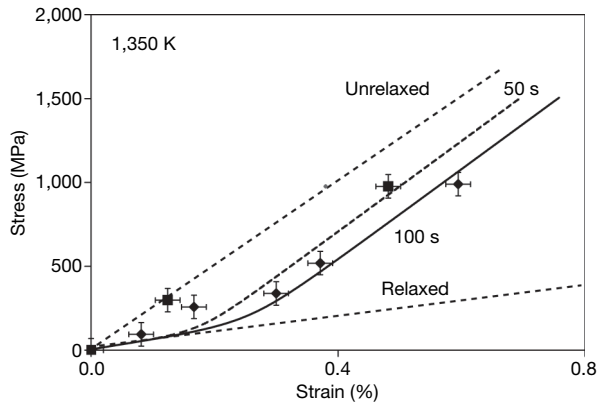


**Figure 4 | Sample stress–strain relationship at 1,350 K.** The samples contain olivine and ringwoodite in about equal proportions. The plotted curves are models for 50-s (squares), 100-s (diamonds), infinitely long (relaxed) and infinitely short (unrelaxed) sampling times. The curves are calculated using the analysis<sup>13</sup> for a two-phase mixture, with adjustments made to reflect a cycling uniaxial stress and parameters of grain size 10  $\mu\text{m}$  and diffusion coefficient  $10^{-15} \text{ m}^2 \text{ s}^{-1}$ . Run number 28; error bars, 1 s.d.

The energy loss for the mixed-phase region is considerably larger than that for the single-phase region, as expected in this model. We again emphasize that the small stress amplitude in the seismic wave may lower the characteristic time to a much smaller value and, thus, shift the attenuation peak to much higher frequencies than those sampled by seismic waves.

The observations suggest a characteristic time on the order of 1,000 s in the laboratory for gigapascal-level stresses. This phenomenon will be important in the seismic record if the characteristic time scales with stress amplitude as suggested by the model outlined above. We tested this scaling by measuring stress and strain as a function of the stress amplitude at fixed frequencies. Figure 4 compares the model predictions for stress amplitude versus strain amplitude with the results for sinusoidal oscillations with 50-s and 100-s periods. For any strain amplitude, the characteristic time  $\tau_1$  was derived in accordance with the discussion above and the stress was calculated using the relaxed modulus, the unrelaxed modulus, the characteristic time and the frequency of the oscillation, according to standard relaxation models<sup>1</sup>. The slope of the stress–strain curve for large-amplitude oscillations is equal to the unrelaxed Young's modulus, whereas the slope at small amplitude reflects the relaxed modulus. The data were constrained to go through the origin. The 50-s model curve has a smaller amount of relaxed strain than the 100-s curve because the transformed sample volume ( $\delta V$ ) is less for shorter transformation times and, hence, shorter periods. Whereas the small-amplitude data exhibit some scatter, the more robust, large-amplitude data are consistent with the model<sup>2</sup> and, therefore, support our claim that the characteristic time decreases as the amplitude of the perturbing stress decreases.

The data presented here imply that phase transitions reduce P-wave velocities in the Earth's mantle. The relaxed and unrelaxed velocities are easy to calculate, but the actual velocity will lie between these values, and the exact amount of softening is not yet known.

Whether or not associated bulk attenuation occurs requires more investigation of the timescales. This suggestion alters the information that is considered essential in creating a seismic profile from mineral physics data. More experiments and directed seismic observations are needed to define the impact of the process presented here.

Received 21 January; accepted 4 July 2008.

- Anderson, D. L. *Theory of the Earth* 279–301 (Blackwell Scientific, 1989).
- Jackson, I. in *Treatise on Geophysics* Vol. 2 (ed. Schubert, G.) 493–525 (Elsevier, 2007).
- Vaisnys, J. R. Propagation of acoustic waves through a system undergoing phase transformations. *J. Geophys. Res.* **73**, 7675–7683 (1968).
- Dziewonski, A. M. & Anderson, D. L. Preliminary reference Earth model. *Phys. Earth Planet. Inter.* **25**, 297–356 (1981).
- Bina, C. R. & Helffrich, G. Phase transition Clapeyron slopes and transition zone seismic discontinuity topography. *J. Geophys. Res.* **99**, 15853–15860 (1994).
- Ringwood, A. E. Phase transformations and the constitution of the mantle. *Phys. Earth Planet. Inter.* **9**, 109–155 (1970).
- Katsura, T. & Ito, E. The system  $\text{Mg}_2\text{SiO}_4\text{-Fe}_2\text{SiO}_4$  at high-pressures and temperatures - precise determination of stabilities of olivine, modified spinel, and spinel. *J. Geophys. Res.* **94**, 15663–15670 (1989).
- Irifune, T. Phase transformations in the Earth's mantle and subducting slabs: Implications for their compositions, seismic velocity and density structures and dynamics. *I. Arc* **2**, 55–71 (1993).
- Akaogi, M., Tanaka, A. & Ito, E. Garnet-ilmenite-perovskite transitions in the system  $\text{Mg}_4\text{Si}_4\text{O}_{12}\text{-Mg}_3\text{Al}_2\text{Si}_3\text{O}_{12}$  at high pressures and high temperatures: phase equilibria, calorimetry and implications for mantle structure. *Phys. Earth Planet. Inter.* **132**, 303–324 (2002).
- Weidner, D. J. & Wang, Y. in *Earth's Deep Interior: Mineral Physics and Tomography from the Atomic to the Global Scale* (eds Karato, S., Forte, A. M., Liebermann, R. C., Masters, G. & Stixrude, L.) 215–235 (American Geophysical Union, 2000).
- Weidner, D. J. & Wang, Y. B. Chemical- and Clapeyron-induced buoyancy at the 660 km discontinuity. *J. Geophys. Res.* **103**, 7431–7441 (1998).
- Brown, J. M. & Shankland, T. J. Thermodynamic parameters in the Earth as determined from seismic profiles. *Geophys. J. R. Astron. Soc.* **66**, 579–596 (1981).
- Chakraborty, S. et al. Enhancement of cation diffusion rates across the 410-kilometer discontinuity in Earth's mantle. *Science* **283**, 362–365 (1999).
- Morris, S. J. S. Coupling of interface kinetics and transformation-induced strain during pressure-induced solid-solid phase changes. *J. Mech. Phys. Solids* **50**, 1363–1395 (2002).
- Tamisiea, M. E. & Wahr, J. M. Phase transitions and short timescale sinusoidal motions. *Earth Planet. Sci. Lett.* **198**, 459–470 (2002).
- Cherniak, D. J. Rare earth element and gallium diffusion in yttrium aluminum garnet. *Phys. Chem. Miner.* **26**, 156–163 (1998).
- Holzappel, C., Rubie, D. C., Frost, D. J. & Langenhorst, F. Fe-Mg interdiffusion in  $(\text{Mg,Fe})\text{SiO}_3$  perovskite and lower mantle reequilibration. *Science* **309**, 1707–1710 (2005).
- Durham, W. B., Weidner, D. J., Karato, S. & Wang, Y. in *Plastic Deformation of Minerals and Rocks* Vol. 51 (eds Karato, S. & Wenk, H.-R.) 21–49 (Mineralogical Society of America, 2002).
- Li, L. & Weidner, D. J. Energy dissipation of materials at high pressure and high temperature. *Rev. Sci. Instrum.* **78**, 053902 (2007).
- Rubie, D. C. & Ross, C. R. Kinetics of the olivine-spinel transformation in subducting lithosphere - experimental constraints and implications for deep slab processes. *Phys. Earth Planet. Inter.* **86**, 223–241 (1994).

**Acknowledgements** We thank L. Wang and D. Lindsley for support for this project. We acknowledge support from the National Synchrotron Light Source and the Consortium for Materials Properties in Earth Sciences, and financial support from the US Department of Energy (contract number DE-ACO2\_98CH10886) and the US National Science Foundation (awards EAR-0711365, EAR652887 and EAR 01-35554). This is MPI publication number 466.

**Author Information** Reprints and permissions information is available at [www.nature.com/reprints](http://www.nature.com/reprints). Correspondence and requests for materials should be addressed to L.L. (lilli@ic.sunysb.edu).